Testing leptoquark and Z' models via $B \to K_1(1270,1400)\mu^+\mu^-$ decays

Zhuo-Ran Huang,[1,*] Muhammad Ali Paracha,[2,1,†] Ishtiaq Ahmed,[3,‡] and Cai-Dian Lü[1,4,§]

[1]*Institute of High Energy Physics, Chinese Academy of Sciences, Beijing 100049, China*
[2]*Department of Physics, School of Natural Sciences (SNS), National University of Sciences and Technology (NUST), Sector H-12, Islamabad 44000, Pakistan*
[3]*National Centre for Physics, Quaid-I-Azam University, Islamabad 45320, Pakistan*
[4]*School of Physics, University of Chinese Academy of Sciences, Beijing 100049, China*

(Received 3 February 2019; published 30 September 2019)

The measurements of $R_{K^{(*)}} = \mathcal{B}(B \to K^{(*)}\mu^+\mu^-)/\mathcal{B}(B \to K^{(*)}e^+e^-)$ in recent years have hinted lepton flavor nonuniversality and thus drawn widespread attentions. If these anomalies are induced by new physics (NP), deviations from the SM predictions may also be found in other channels via the same process at the quark level. In this work, we study in $B \to K_1(1270, 1400)\mu^+\mu^-$ decays the effects of two popular classes of NP models which can address the $b \to s$ anomalies, i.e., the leptoquark models and the Z' models. By assuming that NP only affects the $b \to s\mu^+\mu^-$ transition, we find that the unpolarized and polarized lepton flavor universality (LFU) ratios $R_{K_1^{(L,T)}(1270)}$ are useful to distinguish among the NP models (scenarios) and the SM because they are sensitive to the NP effects and insensitive to the mixing angle θ_{K_1}, while the $R_{K_1^{(L,T)}(1400)}$ are sensitive to both NP and θ_{K_1}. Another ratio $R_\mu(K_1) = \mathcal{B}(B \to K_1(1400)\mu^+\mu^-)/\mathcal{B}(B \to K_1(1270)\mu^+\mu^-)$ is shown to depend weekly on the effects from the NP models (scenarios) under consideration, and thus can be used to determine the θ_{K_1} and complement the $R_{K_1^{(L,T)}}$ in the probe for NP.

DOI: 10.1103/PhysRevD.100.055038

I. INTRODUCTION

In the past few years, several anomalies in B physics [1,2] have been heatedly discussed in the high-energy physics community since these measurements are hints of new physics beyond the Standard Model (SM) or more precisely, the lepton flavor universality violation (LFUV). The *BABAR* Collaboration [3,4] first reported one class of such anomalies, in the measurement of

$$R_{D^{(*)}} = \frac{\mathcal{B}(B \to D^{(*)}\tau\bar{\nu})}{\mathcal{B}(B \to D^{(*)}\ell\bar{\nu})}. \tag{1}$$

The main advantage of considering such a ratio is that it cancels exactly the Cabibbo-Kobayashi-Maskawa matrix (CKM) elements and the uncertainties due to the transition form factors are also partially but largely cancelled. Later on Belle [5–7] and LHCb [8–11] measured the same ratio and also observed the excess: the measured value of $R_{D^*}^{\rm exp}$ is greater than $R_{D^{(*)}}^{\rm SM}$ prediction. The most recent values of $R_{D^{(*)}}$ given by the Heavy Flavor Averaging Group (HFLAV) [12] are

$$R_D = 0.407(46), \qquad R_{D^*} = 0.306(15), \tag{2}$$

The difference between the SM predictions [13–19] and experimental values is approximately 3–4σ and thus gives a hint of NP.

Apart from the tree-level charged current semileptonic B decays, the loop-level rare B decays mediated by the flavor-changing neutral current (FCNC) transition $b \to s\ell^+\ell^-$ also give hints of lepton flavor nonuniversality. Such measurements include the LFU ratios

$$R_{K^{(*)}} = \frac{\int_{q^2_{\rm min}}^{q^2_{\rm max}} \frac{d\mathcal{B}(B\to K^{(*)}\mu^+\mu^-)}{dq^2} dq^2}{\int_{q^2_{\rm min}}^{q^2_{\rm max}} \frac{d\mathcal{B}(B\to K^{(*)}e^+e^-)}{dq^2} dq^2}, \tag{3}$$

and the values reported by LHCb in different bins are [20,21]

$$\begin{aligned} R_K^{[1,6]} &= 0.745^{+0.090}_{-0.074} \pm 0.036, \\ R_{K^*}^{[0.045,1.1]} &= 0.66^{+0.11}_{-0.07} \pm 0.03, \\ R_{K^*}^{[1.1,6]} &= 0.69^{+0.11}_{-0.07} \pm 0.05, \end{aligned} \tag{4}$$

*huangzr@ihep.ac.cn
†aliparacha@sns.nust.edu.pk
‡ishtiaqmusab@gmail.com
§lucd@ihep.ac.cn

of which the tensions with the SM predictions are respectively 2.6σ, 2.1–2.3σ and 2.6σ [22]. These ratios have theoretical uncertainties that are almost canceled (less than 1% [23]), making them very clean probe for NP/LFUV [24]. Although in principal NP is possible to affect both $b \to se^+e^-$ and $b \to s\mu^+\mu^-$, in many existing studies [25–32] the assumption that NP only affects $b \to s\mu^+\mu^-$ has been considered because several other deviations from the SM in $b \to s\mu^+\mu^-$ have been observed [33–35] and the measured branching fraction of $B \to Ke^+e^-$ is consistent with the SM prediction.

Among the NP models that can explain the $b \to s\mu^+\mu^-$ data are leptoquark models [36–44] and Z' models [45–50]. In the language of the effective field theory, these NP models can modify the Wilson coefficients so that the effective Hamiltonian fulfills one of the three possible model-independent NP scenarios that can explain the $b \to s\mu^+\mu^-$ data [30]. If these NP models or model-independent explanations depict the NP in $b \to s\mu^+\mu^-$ at the quark level, one naturally expects to observe similar anomalies in other rare decays such as $B \to K_1\mu^+\mu^-$.[1] In this work, we extent the study of the NP in $b \to s\mu^+\mu^-$ to axial-vector final state mesons, i.e., the K_1 states, which should be useful to test the existing model-independent and model explanations of the $b \to s\mu^+\mu^-$ anomalies. In this context $B \to K_1(1270, 1400)\ell^+\ell^-$ decays are prosperous in phenomenology [53–62] as the physical states $K_1(1270)$ and $K_1(1400)$ are mixture of $^3P_1$ and $^1P_1$ states K_{1A} and K_{1B}:

$$|K_1(1270)\rangle = |K_{1A}\rangle \sin\theta_{K_1} + |K_{1B}\rangle \cos\theta_{K_1}, \quad (5)$$

$$|K_1(1400)\rangle = |K_{1A}\rangle \cos\theta_{K_1} - |K_{1B}\rangle \sin\theta_{K_1}. \quad (6)$$

The mixing angle θ_{K_1} has not been precisely determined, and it was estimated to be $-(34 \pm 13)°$ from the decay $B \to K_1(1270)\gamma$ and $\tau \to K_1(1270)\nu_\tau$ [53]. Therefore in this work we consider different possibilities for θ_{K_1}.

It has been found in articles and also by our independent study that the observables like the branching ratio, the different polarization and angular observables, and also the LFU ratios for semileptonic B meson decays are greatly influenced in different NP models. However predictions for many of these observables can have large theoretical uncertainties, which makes it more involved to distinguish NP. Hence in this work we mainly concentrate on the LFU ratios R_{K_1}, for both unpolarized and polarized K_1 final states. Numerically we use the Wilson coefficients and the NP parameters in Z' and leptoquark models obtained from the fits to the $b \to s\mu^+\mu^-$ data (including the branching fractions and the angular observables for $B \to K^*\mu^+\mu^-$ and $B_s \to \phi^*\mu^+\mu^-$ as well as the $R_{K^{(*)}}$) in [25] to provide with predictions for the LFU ratios, which can be tested by future experiments to dig out the status of NP/LFUV. Since some of the obtained ratios are sensitive to θ_{K_1}, as a complementary study of NP we also perform an analysis of the ratio $R_\mu(K_1) = \mathcal{B}(B \to K_1(1400)\mu^+\mu^-)/\mathcal{B}(B \to K_1(1270)\mu^+\mu^-)$ that has been found to be insensitive to the NP effects from a single NP operator [54], which could be useful to determine the mixing angle.

The organization of the paper is as follows. In Sec. II we present the theoretical formalism in the language of the effective field theory, including giving a brief review of the model-independent NP scenarios, the leptoquark models and the Z' models. In Secs. III and IV, we respectively describe the hadronic form factors adopted in this work and the physical observables. In Sec. V, we present our predictions for different unpolarized and polarized ratios. At last in Sec. VI we give our summary and conclusions.

II. THEORETICAL TOOLKIT

In this section we briefly discuss the theoretical setup and new physics models to analyze the physical observables in $B_d^0 \to K_1(1270, 1400)\mu^+\mu^-$ decays, more precisely we focus our attention on lepton flavor universality parameters for both polarized and unpolarized final state axial vector meson $K_1(1270, 1400)$.

The basic ingredient to do phenomenology in rare decays is the effective Hamiltonian, which for the $b \to s\mu^+\mu^-$ process at the quark level can be written as

$$H_{\text{eff}} = -\frac{4G_F}{\sqrt{2}} V_{tb}V_{ts}^* \Bigg[\sum_{i=1}^{6} C_i(\mu)O_i(\mu) + \sum_{i=7,9,10} C_i(\mu)O_i(\mu) + C_i'(\mu)O_i'(\mu)\Bigg]. \quad (7)$$

The effective Hamiltonian given in Eq. (7) contains the four quark and electromagnetic operators O_i, and $C_i(\mu)$ are their corresponding Wilson coefficients. G_F is the Fermi coupling constant, and V_{tb} and V_{ts}^* are the CKM matrix elements.

The effective operators that contributes both in SM and in NP are summarized as follows

$$O_7 = \frac{e^2}{16\pi^2} m_b(\bar{s}\sigma_{\mu\nu}P_R b)F^{\mu\nu},$$
$$O_9 = \frac{e^2}{16\pi^2}(\bar{s}\gamma_\mu P_L b)(\bar{l}\gamma^\mu l),$$
$$O_{10} = \frac{e^2}{16\pi^2}(\bar{s}\gamma_\mu P_L b)(\bar{l}\gamma^\mu\gamma_5 l), \quad (8)$$

The primed operators given in Eq. (7) are obtained by replacing left-handed fields (L) with right-handed (R) ones. In this work we only consider those scenarios of NP where the operator basis remains the same as that of SM but the Wilson coefficients get modified. The modified Wilson coefficients in the above Hamiltonian can be written as

[1]For studies of the lepton flavor universality in various $b \to s\mu^+\mu^-$ channels, see [51,52].

TABLE I. The Wilson coefficients C_i^μ at the scale $\mu \sim m_b$ in the SM.

C_1	C_2	C_3	C_4	C_5	C_6	C_7	C_9	C_{10}
−0.263	1.011	0.005	−0.0806	0.0004	0.0009	−0.2923	4.0749	−4.3085

$$C_9^{\rm tot} = C_9^{\rm eff} + C_9^{\rm NP} \tag{9}$$

$$C_{10}^{\rm tot} = C_{10}^{\rm SM} + C_{10}^{\rm NP}. \tag{10}$$

The Wilson coefficients incorporate the short distance physics and are evaluated through perturbative approach. The factorizable contributions from current-current, QCD penguins and chromomagnetic operators $O_{1\text{–}6,8}$ have been consolidated in the Wilson coefficients $C_9^{\rm eff}(s)$ and $C_7^{\rm eff}(s)$ and their expressions are given as [63]

$$\begin{aligned} C_7^{\rm eff}(q^2) &= C_7 - \frac{1}{3}\left(C_3 + \frac{4}{3}C_4 + 20C_5 + \frac{80}{3}C_6\right) \\ &\quad - \frac{\alpha_s}{4\pi}[(C_1 - 6C_2)F_{1,c}^{(7)}(q^2) + C_8F_8^7(q^2)] \\ C_9^{\rm eff}(q^2) &= C_9 + \frac{4}{3}\left(C_3 + \frac{16}{3}C_5 + \frac{16}{9}C_6\right) \\ &\quad - h(0,q^2)\left(\frac{1}{2}C_3 + \frac{2}{3}C_4 + 8C_5 + \frac{32}{3}C_6\right) \\ &\quad - \left(\frac{7}{2}C_3 + \frac{2}{3}C_4 + 38C_5 + \frac{32}{3}C_6\right)h(m_b,q^2) \\ &\quad + \left(\frac{4}{3}C_1 + C_2 + 6C_3 + 60C_5\right)h(m_c,q^2) \\ &\quad - \frac{\alpha_s}{4\pi}[C_1F_{1,c}^{(9)}(q^2) + C_2F_{2,c}^{(9)}(q^2) + C_8F_8^{(9)}(q^2)]. \end{aligned} \tag{11}$$

The Wilson coefficients given in Eq. (11) involves the functions $h(m_q, s)$ with $q = c,\ b$ and functions $F_8^{7,9}(q^2)$ are defined in [64] and the function $F_{1,c}^{(7,9}(q^2)$ given in [65] for low q^2 and in [66] for high q^2. The numerical of Wilson coefficents $C_i(i = 1, \ldots\ldots\ldots, 10)$ at $\mu \sim m_b$ are presented in Table I.

In the next subsection we give a brief review of different NP-scenarios [25,26,30] which will be used to analyze the physical observables of Rare $B \to K_1(1270, 1400)\mu^+\mu^-$ decay. In SM and in NP, the effective Hamiltonian (7) gives the matrix element for $B \to K_1(1270, 1400)\mu^+\mu^-$ can be written as

$$\begin{aligned} &\mathcal{M}(B \to K_1\mu^+\mu^-) \\ &= \frac{G_F\alpha}{2\sqrt{2}\pi}V_{tb}V_{ts}^*\Big[\langle K_1(k,\varepsilon)|\bar{s}\gamma^\mu(1-\gamma^5)b|B(p)\rangle\{C_9^{\rm tot}(\bar{\mu}\gamma^\mu\mu) \\ &\quad + C_{10}^{\rm tot}(\bar{\mu}\gamma^\mu\gamma^5\mu)\} - 2C_7^{\rm eff}m_b\langle K_1(k,\varepsilon)|\bar{s}i\sigma_{\mu\nu} \\ &\quad \times \frac{q^\nu}{s}(1+\gamma^5)b|B(p)\rangle(\bar{\mu}\gamma^\mu\mu)\Big]. \end{aligned} \tag{12}$$

In the next subsection we give a brief review of different NP-scenarios [25,26,30] which will be used to analyze the physical observables of rare $B \to K_1(1270, 1400)\mu^+\mu^-$ decay.

A. New physics scenarios

From the model-independent analysis performed in Ref. [30], only the following three NP scenarios for $b \to s\mu^+\mu^-$ are allowed by the experimental data assuming real Wilson coefficients:

$$\begin{aligned} &\text{(I)}\ C_9^{\mu\mu}(\text{NP}) < 0, \\ &\text{(II)}\ C_9^{\mu\mu}(\text{NP}) = -C_{10}^{\mu\mu}(\text{NP}) < 0, \\ &\text{(III)}\ C_9^{\mu\mu}(\text{NP}) = -C_9^{\mu\mu'}(\text{NP}) < 0. \end{aligned} \tag{13}$$

Both scenarios (I) and (II) takes part to investigate the status of NP. However the scenario III is rejected because it predicts $R_K = 1$ and it disagrees with the experiment. The simplest possible NP models involve the tree-level exchange of leptoquark(LQ) or Z' boson. It was shown in Ref. [25] that scenario II can arise in LQ or Z'-models, but scenario I is only possible with a Z'. The details containing LQ's and Z' are given in Refs. [36,67–71].

B. Review of the fitting results for the NP Wilson coefficients

1. Model-independent scenarios

In this work we use the Wilson coefficients fitted in [25] to make predictions for the unpolarized and polarized ratios $R_{K_1^{(L,T)}}$. Following the terms in [25], fit-A was obtained using only CP-conserving $b \to s\mu^+\mu^-$ observables and fit-B using both the CP-conserving observables and $R_{K^{(*)}}$. The NP in both fit A and fit B can be accommodated with the Wilson coefficients (WC's) $C_9^{\mu\mu}(\text{NP})$ and $C_{10}^{\mu\mu}(\text{NP})$ and

TABLE II. Model-independent scenario: best-fit values of the WCs (taken to be real) as well as the pull values in fit-A and fit-B [25].

Scenario	WC: fit-A	Pull	WC: fit-B	Pull
(I) $C_9^{\mu\mu}(\text{NP})$	-1.20 ± 0.20	5.0	-1.25 ± 0.19	5.9
(II) $C_9^{\mu\mu}(\text{NP}) = -C_{10}^{\mu\mu}(\text{NP})$	-0.62 ± 0.14	4.6	-0.68 ± 0.12	5.9
(III) $C_9^{\mu\mu}(\text{NP}) = -C_{10}^{\mu\mu'}(\text{NP})$	-1.10 ± 0.18	5.2	-1.11 ± 0.17	5.6

the numerical values of these WC's obtained in [25] are depicted in Table II.

The simplest NP models that can explain the $b \to s\mu^+\mu^-$ anomalies are the tree-level exchange of a new particle such as a leptoquark (LQ) or a Z' boson. The details of the LQ and the Z' models were presented in [25,26] and references therein. However in the next section we briefly discuss those leptoquark and Z' models that can explain the $b \to s\mu^+\mu^-$ data.

2. Leptoquark models

There are ten versions of leptoquarks that couple to the SM particles through dimension ≤ 4 effective operators [37]. Among them, the scalar isotriplet S_3, the vector isosinglet U_1 and the vector isotriplet U_3 respectively with $Y = 1/3$, $Y = -2/3$ and $Y = -2/3$ can explain the $b \to s\mu^+\mu^-$ data [18,26] (and the U_1 can also simultaneously explain the $b \to c$ anomalies [72–75]). The NP in LQ models can be accommodated via the Wilson coefficients, $C_9^{\mu\mu}(NP) = -C_{10}^{\mu\mu}(NP)$. Such type of LQ models fall within the model-independent scenario II given in Eq. (13), thus the best-fit WC's for such LQ models remain the same as those for scenario II presented in Table II. In these models LQ's are generated at the tree level and can be written as

$$C_9^{\mu\mu}(NP) \propto \frac{g_L^{b\mu} g_L^{s\mu}}{M_{\rm LQ}^2}, \tag{14}$$

where $g_L^{b\mu}$ and $g_L^{s\mu}$ are the couplings of the LQ and M_{LQ} is the LQ mass, on which the constraint from the direct search is $M_{LQ} > 640$ GeV [76].

3. Z' models

Like the variety of LQ models, there are also different versions of Z' models [26,36,77]. As discussed in previous sections, the Z' models that can explain the $b \to s\mu^+\mu^-$ anomalies should satisfy the model-independent scenarios I and II. Unlike the leptoquark models which can only be accommodated with scenario II, both I and II can be realized with a Z' exchange. To be general, in [25] both the heavy and light Z' models were considered. Next we briefly review their results.

(A) Heavy Z'

For Z' models of scenario I and II, by integrating out the heavy Z', the effective Lagrangian can be written as

$$\mathcal{L}_{Z'}^{\rm eff} = -\frac{1}{2M_{Z'}^2} J_\mu J^\mu \tag{15}$$

where

$$J^\mu = -g_{LL}^{\mu\mu}\bar{L}\gamma^\mu P_L L + g_R^{\mu\mu}\bar{\mu}\gamma^\mu P_R \mu + g_L^{bs}\bar{\psi}_{q_2}\gamma^\mu P_L \psi_{q_3} + \text{H.c.}$$

In terms of four fermion operators the effective Lagrangian(15) can be expressed as

$$\begin{aligned}\mathcal{L}_{Z'}^{\rm eff} = &-\frac{g_L^{bs}}{M_{Z'}^2}(\bar{s}\gamma^\mu b)(\bar{\mu}\gamma^\mu(g_L^{\mu\mu}P_L + g_R^{\mu\mu}P_R)\mu),\\ &-\frac{(g_L^{bs})^2}{2M_{Z'}^2}(\bar{s}\gamma^\mu P_L b)(\bar{s}\gamma^\mu P_L b),\\ &-\frac{g_L^{\mu\mu}}{M_{Z'}^2}(\bar{\mu}\gamma^\mu(g_L^{\mu\mu}P_L + g_R^{\mu\mu}P_R)\mu)(\bar{\nu}_\mu\gamma^\mu P_L\nu_\mu).\end{aligned} \tag{16}$$

In Eq. (16) the first four-fermion operator is relevant to $b \to s\mu^+\mu^-$ transitions, the second operator makes contribution to the $B_s^0 - \bar{B}_s^0$ mixing and the third operator has effects on the neutrino trident production.

The NP effects in Z' models can modify the WC's

$$\begin{aligned}C_9^{\mu\mu}(\mathbf{NP}) &= -\left[\frac{\pi}{\sqrt{2}G_F\alpha V_{tb}V_{ts}^*}\right]\frac{g_L^{bs}(g_L^{\mu\mu} + g_R^{\mu\mu})}{M_{Z'}^2},\\ C_{10}^{\mu\mu}(\mathbf{NP}) &= \left[\frac{\pi}{\sqrt{2}G_F\alpha V_{tb}V_{ts}^*}\right]\frac{g_L^{bs}(g_L^{\mu\mu} - g_R^{\mu\mu})}{M_{Z'}^2}.\end{aligned} \tag{17}$$

Considering the constraints from the $B_s^0 - \bar{B}_s^0$ mixing and the neutrino trident production, the best-fit values of the couplings g_L^{bs} and $g_{L,R}^{\mu\mu}$ were obtained in [25], which are presented in Tables III and IV.

(B) Light Z'

A light Z' is also possible to address the $b \to s\mu^+\mu^-$ data. Given the absence of any signature for such a state in the dimuon invariant mass, two typical Z' masses, $M_{Z'} = 10$ GeV $> m_B$ and $M_{Z'} = 200$ MeV $< 2m_\mu$ can be considered. The corresponding Z' models are called the GeV Z' model and the MeV Z' model, which respectively has intimation for dark matter [78] and nonstandard neutrino interactions [79]. The MeV Z' model can also explain the muon $g-2$ [79].[2]

For the light Z' models, the vertex $\bar{s}bZ'$ takes the following form [25]

$$F(q^2)\bar{s}\gamma^\mu P_L b Z'_\mu, \tag{18}$$

where for $q^2 \ll m_B^2$, the form factor $F(q^2)$ can be expanded as

$$F(q^2) = a_L^{bs} + g_L^{bs}\frac{q^2}{m_B^2} + \cdots. \tag{19}$$

[2]Recently in [80] it was shown that a heavier family specific Z' may also resolve the muon g-2 anomaly if the chirality flipping effects are carefully considered.

TABLE III. TeV Z' model (scenario I and II); best-fit values of g_L^{bs} in fit-A [25].

$M_{Z'} = 1\mathbf{TeV}$				
$g_L^{\mu\mu}$	$Z'(I): g_L^{bs} \times 10^3$	Pull	$Z'(II): g_L^{bs} \times 10^3$	Pull
0.5	-1.8 ± 0.3	5.0	-1.9 ± 0.4	4.6

TABLE IV. TeV Z' model (scenario I and II); best-fit values of g_L^{bs} in fit-B [25].

$M_{Z'} = 1\mathbf{TeV}$				
$g_L^{\mu\mu}$	$Z'(I): g_L^{bs} \times 10^3$	Pull	$Z'(II): g_L^{bs} \times 10^3$	Pull
0.5	-1.9 ± 0.3	5.9	-2.1 ± 0.4	5.9

TABLE V. GeV Z' model (scenario I and II); best-fit values of a_L^{bs} in fit-A [25].

$M_{Z'} = 10\ \mathbf{GeV}$				
$g_L^{\mu\mu} \times 10^2$	$Z'(I): a_L^{bs} \times 10^6$	Pull	$Z'(II): a_L^{bs} \times 10^6$	Pull
1.2	-5.2 ± 1.2	4.2	-7.2 ± 1.8	4.5

However the GeV Z' model is independent of the form factors, and the vertex factor in this model is a_L^{bs} for all q^2, while for the MeV Z' model, a_L^{bs} is severely constrained by $B \to K\nu\bar{\nu}$ and thus can be neglected. The modified WC's of the MeV and the GeV Z' models for $b \to s\mu^+\mu^-$ are

$$C_9^{\mu\mu}(\mathbf{NP}) = \left[\frac{\pi}{\sqrt{2}G_F\alpha V_{tb}V_{ts}^*}\right] \times \frac{(a_L^{bs} + g_L^{bs}(q^2/m_B^2))(g_L^{\mu\mu} + g_R^{\mu\mu})}{q^2 - M_{Z'}^2},$$
$$C_{10}^{\mu\mu}(\mathbf{NP}) = -\left[\frac{\pi}{\sqrt{2}G_F\alpha V_{tb}V_{ts}^*}\right] \times \frac{(a_L^{bs} + g_L^{bs}(q^2/m_B^2))(g_L^{\mu\mu} - g_R^{\mu\mu})}{q^2 - M_{Z'}^2}. \quad (20)$$

where for the GeV Z' model the numerical values of the coupling a_L^{bs} are given in Table V, which are obtained from fits to the $b \to s\mu^+\mu^-$ data with consideration of the constraint on a_L^{bs} from $B_s^0 - \bar{B}_s^0$ mixing. For the MeV Z' model, $g_L^{\mu\mu} = 10^{-3}$ and $g_L^{bs} = 2.1 \times 10^{-5}$ can be obtained for scenario I from the neutrino trident production constraint plus a fit to the $b \to s\mu^+\mu^-$ data, with pull = 4.4.

III. FORM FACTORS AND MIXING OF $K_1(1270) - K_1(1400)$

The exclusive $B \to K_1(1270, 1400)\mu^+\mu^-$ decays involve the hadronic matrix elements of quark operators, which can be parametrized in terms of the form factors as

$$\langle K_1(k,\epsilon)|V_\mu|B(p)\rangle = \varepsilon_\mu^*(M_B + M_{K_1})V_1(q^2) - (p+k)_\mu(\varepsilon^*.q)\frac{V_2(q^2)}{M_B + M_{K_1}} - q_\mu(\varepsilon^*.q)\frac{2M_{K_1}}{q^2}[V_3(q^2) - V_0(q^2)], \quad (21)$$

$$\langle K_1(k,\epsilon)|A_\mu|B(p)\rangle = -\frac{2i\epsilon_{\mu\nu\alpha\beta}}{M_B + M_{K_1}}\varepsilon^{*\nu}p^\alpha k^\beta A(q^2), \quad (22)$$

where $V^\mu = \bar{s}\gamma^\mu b$ and $A^\mu = \bar{s}\gamma^\mu\gamma^5 b$ are vector and axial vector currents, $\varepsilon^{*\nu}$ are polarization vector of the axial vector meson. The relation for vector form factors in Eq. (21) are

$$V_3(q^2) = \frac{M_B + M_{K_1}}{2M_{K_1}}V_1(q^2) - \frac{M_B - M_{K_1}}{2M_{K_1}}V_2(q^2),$$
$$V_3(0) = V_0(0). \quad (23)$$

The other contributions from the tensor form factors are

$$\langle K_1(k,\epsilon)|\bar{s}i\sigma_{\mu\nu}q^\nu b|B(p)\rangle = [(M_B^2 - M_{K_1}^2)\varepsilon_\mu^* - (\varepsilon^*.q)(p+k)_\mu]T_2(q^2) + (\varepsilon^*.q)\left[q_\mu - \frac{q^2}{M_B^2 - M_{K_1}^2}(p+k)_\mu\right]T_3(q^2), \quad (24)$$

$$\langle K_1(k,\epsilon)|\bar{s}i\sigma_{\mu\nu}q^\nu\gamma^5 b|B(p)\rangle = 2i\epsilon_{\mu\nu\alpha\beta}\varepsilon^{*\nu}p^\alpha k^\beta T_1(q^2). \quad (25)$$

The physical states $K_1(1270)$ and $K_1(1400)$ are mixed states of K_{1A} and K_{1B} with mixing angle θ_K defined as

$$|K_1(1270)\rangle = |K_{1A}\rangle\sin\theta_{K_1} + |K_{1B}\rangle\cos\theta_{K_1}, \quad (26)$$

$$|K_1(1400)\rangle = |K_{1A}\rangle\cos\theta_{K_1} - |K_{1B}\rangle\sin\theta_{K_1}. \quad (27)$$

In terms of K_{1A} and K_{1B}, the matrix element $B \to K_1(1270, 1400)$ can be parametrized in terms of the form factors as

$$\begin{pmatrix}\langle K_1(1270)|\bar{s}\gamma_\mu(1-\gamma_5)b|B\rangle \\ \langle K_1(1400)|\bar{s}\gamma_\mu(1-\gamma_5)b|B\rangle\end{pmatrix} = M\begin{pmatrix}\langle K_{1A}|\bar{s}\gamma_\mu(1-\gamma_5)b|B\rangle \\ \langle K_{1B}|\bar{s}\gamma_\mu(1-\gamma_5)b|B\rangle\end{pmatrix}, \quad (28)$$

$$\begin{pmatrix}\langle K_1(1270)|\bar{s}\sigma_{\mu\nu}q^\nu(1+\gamma_5)b|B\rangle \\ \langle K_1(1400)|\bar{s}\sigma_{\mu\nu}q^\nu(1+\gamma_5)b|B\rangle\end{pmatrix} = M\begin{pmatrix}\langle K_{1A}|\bar{s}\sigma_{\mu\nu}q^\nu(1+\gamma_5)b|B\rangle \\ \langle K_{1B}|\bar{s}\sigma_{\mu\nu}q^\nu(1+\gamma_5)b|B\rangle\end{pmatrix}, \quad (29)$$

where the mixing matrix M can be written as

TABLE VI. $B \to K_{1A,1B}$ form factors [54], where a and b are the parameters of the form factors in dipole parametrization.

$\mathcal{T}_i^X(q^2)$	$\mathcal{T}(0)$	a	b	$\mathcal{T}_i^X(q^2)$	$\mathcal{T}(0)$	a	b
$V_1^{K_{1A}}$	0.34	0.635	0.211	$V_1^{K_{1B}}$	−0.29	0.729	0.074
$V_2^{K_{1A}}$	0.41	1.51	1.18	$V_1^{K_{1B}}$	−0.17	0.919	0.855
$V_0^{K_{1A}}$	0.22	2.40	1.78	$V_0^{K_{1B}}$	−0.45	1.34	0.690
$A^{K_{1A}}$	0.45	1.60	0.974	$A^{K_{1B}}$	−0.37	1.72	0.912
$F_1^{K_{1A}}$	0.31	2.01	1.50	$F_1^{K_{1B}}$	−0.25	1.59	0.790
$F_2^{K_{1A}}$	0.31	0.629	0.387	$F_2^{K_{1B}}$	−0.25	0.378	−0.755
$F_3^{K_{1A}}$	0.28	1.36	0.720	$F_3^{K_{1B}}$	−0.11	1.61	10.2

$$M = \begin{pmatrix} \sin\theta_K & \cos\theta_K \\ \cos\theta_K & -\sin\theta_K \end{pmatrix}. \tag{30}$$

The form factors used in the analysis of physical observables were calculated in the framework of QCD light cone sum rules. These results are applicable only at low q^2 region. However to investigate the effects of observables on the whole kinematical region, the form factors can be parametrized in the three-parameter form as [54][3]

$$\mathcal{T}_i^X(q^2) = \frac{\mathcal{T}_i^X(0)}{1 - a_i^X(q^2/m_B^2) + b_i^X(q^2/m_B^2)^2}, \tag{31}$$

where $\mathcal{T}$ is A, V or F form factors and the subscript i can take a value 0, 1, 2, or 3, and the superscript X denotes the K_{1A} or K_{1B} states. The numerical results of form factors at $q^2 = 0$ are presented in Table VI.

IV. LFU RATIOS $R_{K_1^{(L,T)}}$ AND RATIO $R_\mu(K_1)$

In this section we present the formalism for the LFU ratios R_{K_1} and the ratio $R_\mu(K_1)$, considering unpolarized and polarized (longitudinal and transverse) final state axial-vector mesons $K_1(1270, 1400)$, and their sensitivity for different NP scenarios (scenario I and scenario II) or NP models (leptoquark models and heavy and light Z' models). The R_{K_1} parameter is a good tool to investigate NP, as the form factors in this observable is almost cancels out. We now define unpolarized and polarized LFU ratios as:

$$R_{K_1^{(L,T)}(1270,1400)}(q^2) = \frac{d\mathcal{B}(B \to K_1^{(L,T)}(1270, 1400)\mu^+\mu^-)/dq^2}{d\mathcal{B}(B \to K_1^{(L,T)}(1270, 1400)e^+e^-)/dq^2}. \tag{32}$$

Since K_1 meson involves the mixing angle θ_{K_1}, therefore to determine the mixing angle θ_{K_1}, we define another ratio R_μ for K_1 mesons as

$$R_\mu(K_1^{(L,T)})(q^2) = \frac{d\mathcal{B}(B \to K_1^{(L,T)}(1400)\mu^+\mu^-)/dq^2}{d\mathcal{B}(B \to K_1^{(L,T)}(1270)\mu^+\mu^-)/dq^2}. \tag{33}$$

To compute the above ratios we use the amplitude for the $B \to K_1\mu^+\mu^-$ decays given in Eq. (12).

The matrix element given in Eq. (12) can also be written as

$$\mathcal{M} = \frac{G_F\alpha}{2\sqrt{2}\pi}\lambda_t\{T_1^\mu\bar{\mu}\gamma_\mu\mu + T_2^\mu\bar{\mu}\gamma_\mu\gamma_5\mu\} \tag{34}$$

where the form factors and Wilson coefficients are hidden in T_i^μ which can be expressed as follows:

$$T_i^\mu = T_i^{\mu\nu}\varepsilon_\nu^*(i = 1, 2) \tag{35}$$

and

$$T_{1\mu\nu} = \{-i\epsilon_{\mu\nu\alpha\beta}p^\alpha k^\beta\mathcal{F}_1(q^2) - g_{\mu\nu}\mathcal{F}_2(q^2) + P_\mu q_\nu\mathcal{F}_3(q^2) + q_\mu q_\nu\mathcal{F}_4(q^2)\}, \tag{36}$$

$$T_{2\mu\nu} = \{-i\epsilon_{\mu\nu\alpha\beta}p^\alpha k^\beta\mathcal{F}_5(q^2) - g_{\mu\nu}\mathcal{F}_6(q^2) + P_\mu q_\nu\mathcal{F}_7(q^2) + q_\mu q_\nu\mathcal{F}_8(q^2)\},, \tag{37}$$

where the auxiliary functions $\mathcal{F}_1, \ldots\ldots, \mathcal{F}_8$ accommodate both the form factors and Wilson coefficients. The explicit expressions for them can be written as follows

$$\begin{aligned}
\mathcal{F}_1(q^2) &= 2C_9^{\rm tot}\frac{A(q^2)}{M_B + M_{K_1}} + \frac{4m_b}{q^2}C_7^{\rm eff}T_1(q^2),\\
\mathcal{F}_2(q^2) &= C_9^{\rm tot}(M_B + M_{K_1})V_1(q^2) + \frac{2m_b}{q^2}C_7^{\rm eff}(M_B^2 - M_{K_1}^2)T_2(q^2),\\
\mathcal{F}_3(q^2) &= C_9^{\rm tot}\frac{V_2(q^2)}{M_B + M_{K_1}} - \frac{2m_b}{q^2}C_7^{\rm eff}\left(T_2(q^2) - \frac{q^2}{M_B^2 - M_{K_1}^2}T_3(q^2)\right),\\
\mathcal{F}_4(q^2) &= C_9^{\rm tot}\frac{2M_{K_1}}{q^2}[V_3(q^2) - V_0(q^2)] - \frac{2m_b}{q^2}C_7^{\rm eff}T_3(q^2),
\end{aligned} \tag{38}$$

[3]The choice of the hadronic form factors makes very tiny difference in the analysis due to the fact that the form factors in the LFU ratios essentially cancel.

and also

$$\mathcal{F}_5(q^2) = 2C_{10}^{\rm tot}\frac{A(q^2)}{M_B + M_{K_1}},$$
$$\mathcal{F}_6(q^2) = C_{10}^{\rm tot}(M_B + M_{K_1})V_1(q^2),$$
$$\mathcal{F}_7(q^2) = C_{10}^{\rm tot}\frac{V_2(q^2)}{M_B + M_{K_1}},$$
$$\mathcal{F}_8(q^2) = C_{10}^{\rm tot}\frac{2M_{K_1}}{q^2}[V_3(q^2) - V_0(q^2)]. \quad (39)$$

Since the final state mesons $K_1(1270)$ and $K_1(1400)$ involve the mixing angle θ_K, the form factors of $K_1(1270, 1400)$ in Eqs. (38) and (39) can be written in terms of the form factors of K_{1A} and K_{1B}: $B \to K_1(1270)$ form factors in terms of mixing angle θ_K

$$A(q^2) = -A^{K_{1A}}\sin\theta_K + A^{K_{1B}}\cos\theta_K,$$
$$V_i(q^2) = -V_i^{K_{1A}}\sin\theta_K + V_i^{K_{1B}}\cos\theta_K,$$
$$F_i(q^2) = -F_i^{K_{1A}}\sin\theta_K + F_i^{K_{1B}}\cos\theta_K. \quad (40)$$

$B \to K_1(1400)$ form factors in terms of mixing angle θ_K

$$A(q^2) = A^{K_{1A}}\cos\theta_K - A^{K_{1B}}\cos\theta_K,$$
$$V_i(q^2) = V_i^{K_{1A}}\cos\theta_K - V_i^{K_{1B}}\sin\theta_K,$$
$$F_i(q^2) = F_i^{K_{1A}}\cos\theta_K - F_i^{K_{1B}}\sin\theta_K. \quad (41)$$

V. PHENOMENOLOGICAL ANALYSIS OF $R_{K_1^{(L,T)}}$ AND $R_\mu(K_1)$

In this section, we give predictions for the unpolarized and polarized LFU ratios $R_{K_1^{(L,T)}}$[4] in the SM and in the NP models under consideration. In the numerical calculation, we adopt the following input parameters [82]:

$$m_B = 5.28\ \text{GeV}, \quad m_b = 4.18\ \text{GeV}, \quad m_\mu = 0.105\ \text{GeV},$$
$$m_\tau = 1.77\ \text{GeV}, \quad f_B = 0.25\ \text{GeV}, \quad |V_{tb}V_{ts}^*| = 41 \times 10^{-3},$$
$$\alpha^{-1} = 137, \quad G_F = 1.17 \times 10^{-5}\ \text{GeV}^{-2}, \quad \tau_B = 1.54 \times 10^{-12}\ \text{s},$$
$$m_{K_1(1270)} = 1.270\ \text{GeV}, \quad m_{K_1(1400)} = 1.403\ \text{GeV}.$$

To obtain the results in the model-independent scenarios, the Wilson coefficients given in Table II are used. As mentioned previously, the model-independent Wilson coefficients in Scenario II can also be achieved in the leptoquark models, therefore the corresponding predictions also represent the results in the leptoquark models. For Z' models, we obtain our predictions using the couplings listed in Tables III–IV. We present the results obtained in different NP models and NP scenarios in separate plots, but one will see that the major factor that affects the predictions are the NP scenario I and II rather than the specific NP models which means the plots corresponding to the leptoquark, heavy and light Z' models are similar once they fulfill the same NP scenario. This is not surprising because from Tables II–V one sees the pull values for the same NP scenario (but in different NP models) are close, which means the leptoquark models and Z' models can reproduce or nearly reproduce the model-independent results under current experimental constraints. Furthermore, since the K_1 mixing angle has not been precisely determined, to be more general, we also consider different possibilities of the K_1 mixing angle [53,54] in our analysis.

In the figures of this section we plot the physical observables in low and high q^2 regions, as we already discussed in Sec. II the functions $F_8^{7,9}(q^2)$ and $F_{1c}^{7,9}(q^2)$ involved in the definition of Wilson coefficents $C_7^{\rm eff}(q^2)$ and $C_7^{\rm eff}(q^2)$ given in Eq. (11) defined for low and high q^2 separately. To provide a comparison with future experimental results, the LFU ratios in low and high q^2 bins are presented in Appendix A.

In Fig. 1, we have plotted the LFU parameter $R_{K_1(1270)}$ against the square of the momentum transfer q^2 in the SM and in different NP models under consideration. One can see that for a given q^2 region, the impact of the NP on this observable is distinct from the SM value which is ≈1. It can also be noticed that the value of $R_{K_1(1270)}$ in low q^2 region decreases when the value of q^2 increases. However, in the region above $q^2 = 4\ \text{GeV}^2$ the observable $R_{K_1(1270)}$ does not vary with the value of q^2. This figure also shows that the variation in the values of $R_{K_1(1270)}$ due to the different NP models are almost the same. However, as compared to the SM, the behavior of $R_{K_1(1270)}$ due to scenario I and scenario II are clearly distinguishable. This suggests that the

[4]Comparison of $R_{K^{(*)}}$, R_{K_0} and R_{K_1} and detailed discussions based on symmetries can be found in [81].

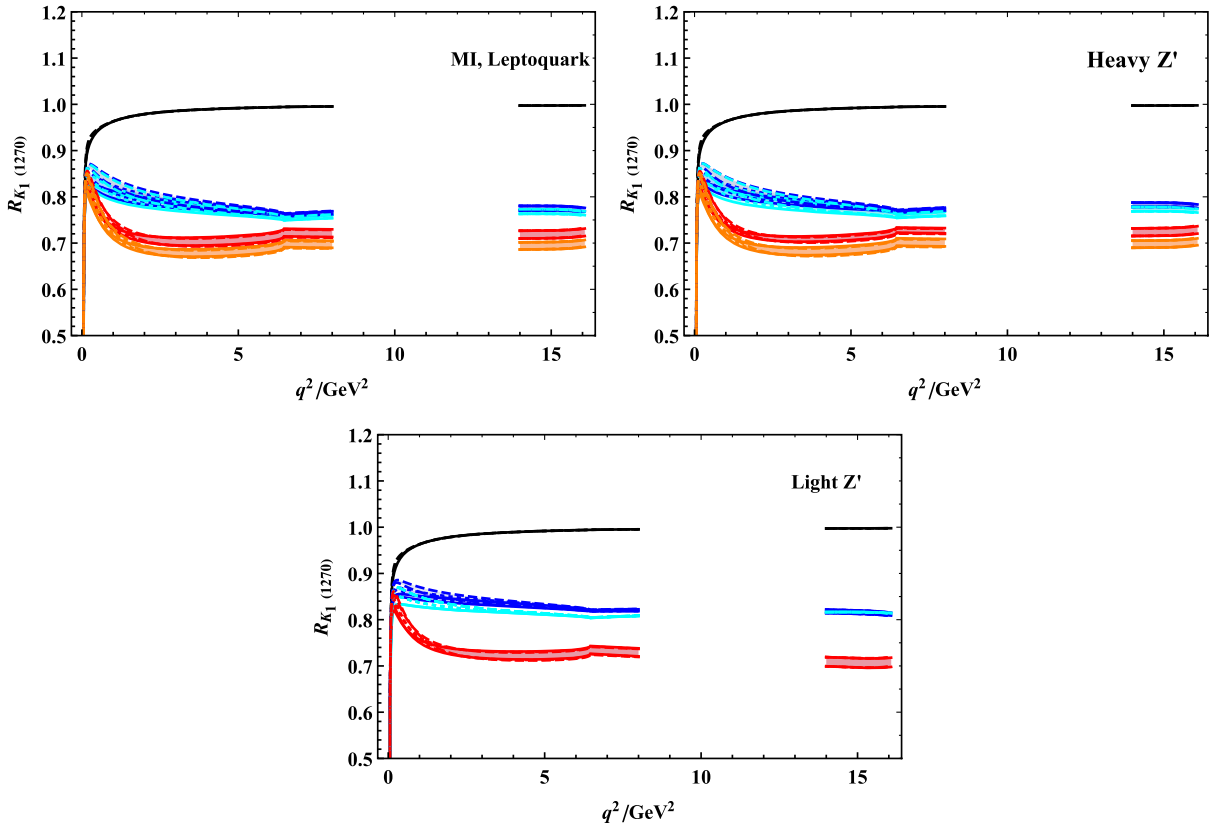

FIG. 1. The Standard Model, model-independent scenarios, leptoquark models, and heavy and light Z' models predictions for the LFU ratio $R_{K_1(1270)}$. The black curves denote the predictions in the SM, the blue, cyan, red, and orange bands show the predictions obtained in scenario I(A), I(B), II(A), and II(B), respectively, including the errors due to errors of the modified Wilson coefficients. For each scenario, the bands with solid, dotted, and dashed boundary curves correspond to $\theta_{K_1} = -34°, -45°, -57°$, respectively. The results in scenario II(A) and II(B) also represent the predictions from the leptoquark models.

precise measurement of $R_{K_1(1270)}$ in current and future colliders will segregate the SM from the leptoquark and the Z' models. Moreover if scenario I is observed, it can only be realized in Z' models.

Similarly, in Fig. 2, we have plotted the polarized LFU parameters $R_{K_1^{L,T}(1270)}$ (i.e., the ratio when K_1 meson is longitudinally or transversely polarized) against the square of the momentum transfer q^2 in the SM and in the different NP models. This figure also represent that the NP effects are quite distinguishable. For the case of the longitudinal LFU parameter $R_{K_1^L(1270)}$ it is shown that by increasing the value of q^2, the behavior of the observable $R_{K_1^L(1270)}$ remains stable in both scenario-I and scenario-II for all NP models under consideration. However the values of $R_{K_1^L(1270)}$ in scenario-I and scenario-II are distinguishable and are approximately 0.75 to 0.80 and 0.65 to 0.70 respectively. Furthermore on the right panel of Fig. 2 one can see the value of the transverse LFU parameter $R_{K_1^T(1270)}$ does vary at low q^2 region, i.e., around $q^2 = 1$–2 GeV^2, the value of $R_{K_1^T(1270)}$ exceeds 1 for all NP models under discussion. Therefore, these polarized observables, particularly the $R_{K_1^T(1270)}$ in low q^2 region are useful to probe the effects of a leptoquark or a Z' Model.

For the sake of completeness and complementarity, we would also like to see the influence of NP on the values of the LFU parameters when the final state axial vector meson is $K_1(1400)$, which is an axial partner of the $K_1(1270)$. Before presenting the results for polarized and unpolarized LFU parameters $R_{K_1^{(L,T)}}(1400)$, we need to recall that $\mathcal{B}(B \to K_1(1400)\mu^+\mu^-)$ is 1–2 orders of magnitude suppressed as compared with $\mathcal{B}(B \to K_1(1270)\mu^+\mu^-)$ $(\sim 10^{-7})$. This suppression arises due to the transformation of the transition form factors for $B \to K_1(1400)\mu^+\mu^-$ decay, differently than the $B \to K_1(1270)\mu^+\mu^-$ decay, and was already shown in Eqs. (40), (41) and Refs. [53,54]. However our results in Figs. 3 and 4 for unpolarized and polarized LFU parameters $R_{K_1^{(L,T)}(1400)}$ show even more interesting behaviors. In Fig. 3, one can see that when $\theta_{K_1} = -34°$ $R_{K_1(1400)}$ shows more variance and can exceed one

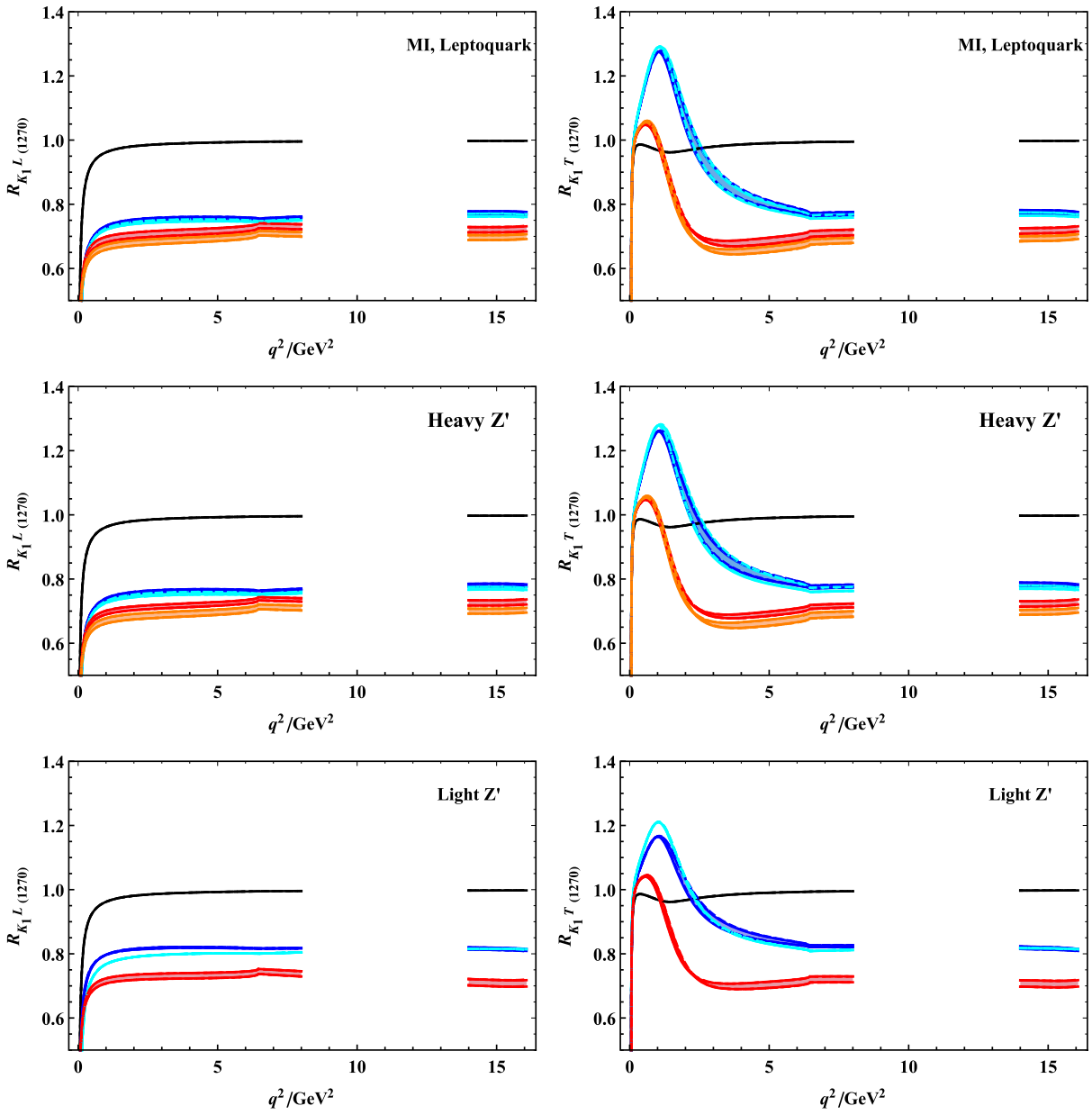

FIG. 2. Predictions for the polarized LFU ratios $R_{K_1^{(L,T)}(1270)}$ in the SM, model-independent scenarios, leptoquark, heavy and light Z' models. The legends are the same as in Fig. 1.

(for scenario I) in low q^2 region.[5] However for $\theta_{K_1} = -45°$ and $-57°$ the $R_{K_1(1400)}$ does not show much variation as depicted by bands with dotted and dashed boundary lines in Fig. 3. The behaviors of $R_{K_1(1400)}$ are quite distinctive for scenario-I and II corresponding to the NP models under consideration.

For the polarized LFU parameters $R_{K_1^{L,T}(1400)}$, the results are depicted in Fig. 4. It shown that $R_{K_1^L(1400)}$ is very sensitive to NP, and very interestingly, we have found two peaks in its value, nearly at 8 GeV^2 slightly below the J/ψ resonance and at 14.5 GeV^2. These peaks arises due to the transformation of transition form factors for $B \to K_1(1400)$. The peak around $q^2 = 7$ GeV^2 comes when we set the value of mixing angle $-34°$ as denoted by the solid lines and this peak shifts ahead to around $q^2 = 14.5$ GeV^2 when $\theta_{K_1} = -45°$ as denoted by the dotted lines. At the value of $\theta_{K_1} = -57°$ this peak goes further away. Therefore our analysis shows that for the observable $R_{K_1^L(1400)}$, the position of this peak strongly depends on the value of the mixing angle θ_{K_1}. Therefore,

[5]Note that $R_{K_1(1400)}$ is very tiny near the maximum hadronic recoil point as shown in Fig. 3, which result in the binned values less than 1 as listed in Table VIII.

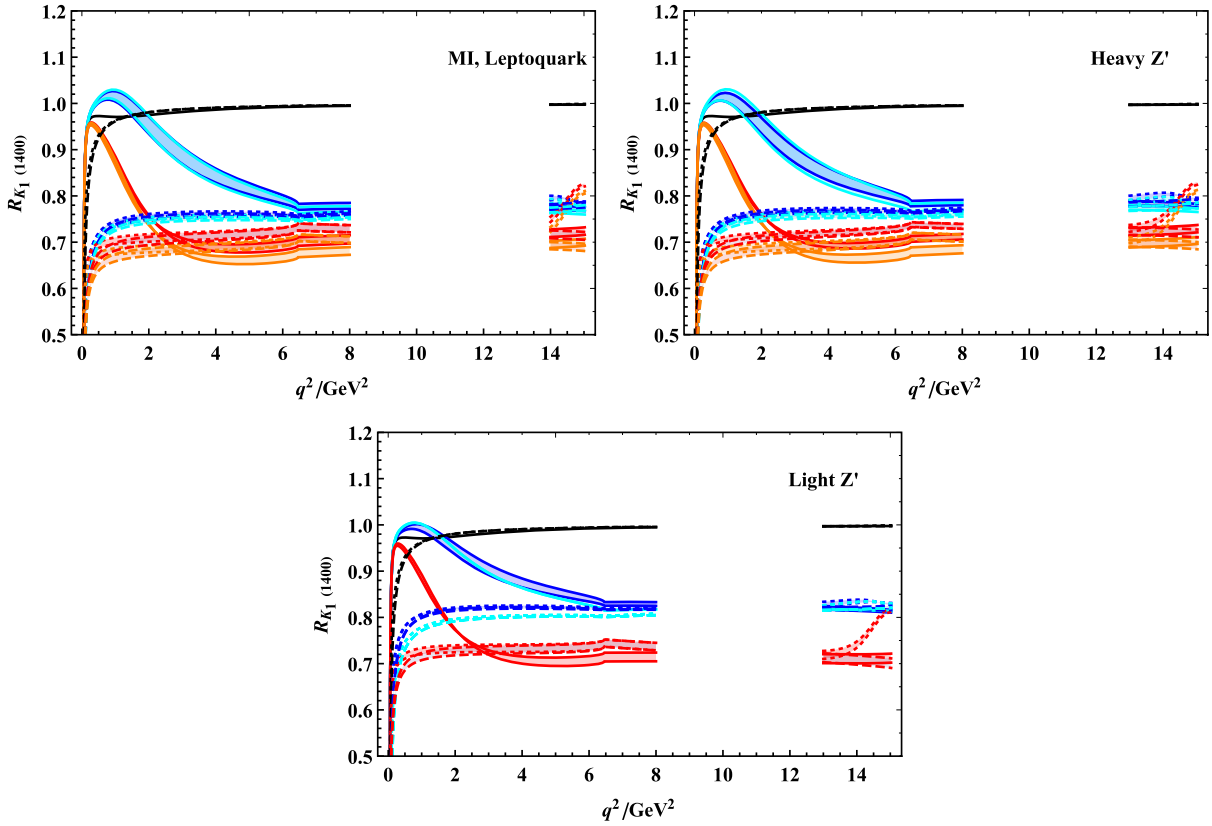

FIG. 3. Predictions for the polarized LFU ratios $R_{K_1(1400)}$ in the Standard Model, model-independent scenarios, leptoquark models, heavy and light Z' models. The legends are the same as in Fig. 1.

the measurement of the value of $R_{K_1^L(1400)}$ can be used to study the mixing angle. Similar to $R_{K_1^T(1270)}$ the value of $R_{K_1^T(1400)}$ is also sensitive to NP, however, this observable is more sensitive to the mixing angle θ_{K_1} as shown in Fig. 4.

As can be seen in Figs. 3 and 4, the LFU parameters for $K_1(1400)$ are sensitive to θ_{K_1} in the NP scenarios/models under consideration. To better study the NP effects, one needs other observables that can determine the K_1 mixing angle. As mentioned earlier, the ratio $R_\mu(K_1)$ is possible to be such an observable, since it has already been shown to be insensitive to the NP effects from a single NP operator [54]. This character also hold for more complicated NP scenarios as well as the leptoquark and the Z' models. In Fig. 5, we present our results for the unpolarized and the polarized R_μ in the model-independent scenario I and II (those for leptoquark and Z' models are quite similar as we have explained). These ratios are again insensitive to the NP effects: the curves of the same type with different colors almost overlap with each other. The unpolarized, longitudinal and transverse ratios R_μ can be used to determine θ_{K_1} and thus are complementary to the LFU ratios in testing the NP effects from the leptoquark and the Z' models.

VI. SUMMARY AND CONCLUSIONS

Motivated by the experimental hints of the lepton universality flavor violation in the flavor-changing neutral current B decays, namely the $R_{K^{(*)}}$ anomalies, we calculate the values of unpolarized and polarized lepton flavor universality ratios $R_{K_1(1270,1400)}$ and $R_{K_1^{L,T}(1270,1400)}$ in the range of low and high q^2. Due to the cancellation of the hadronic uncertainties, these observables are suitable for investigating the NP effects.

In our study, by assuming that the NP only have effects in the $b \to s\mu^+\mu^-$ transition but does not in the $b \to se^+e^-$ transition, we consider different extensions of the SM, including the model-independent scenario I and II required by the current $b \to s\mu^+\mu^-$ measurements, leptoquark models and heavy and light Z' models which can also satisfy scenario I and II. We use the recent constraints on the parametric values of the models under consideration to study how the values of the observables, mentioned above, change under the

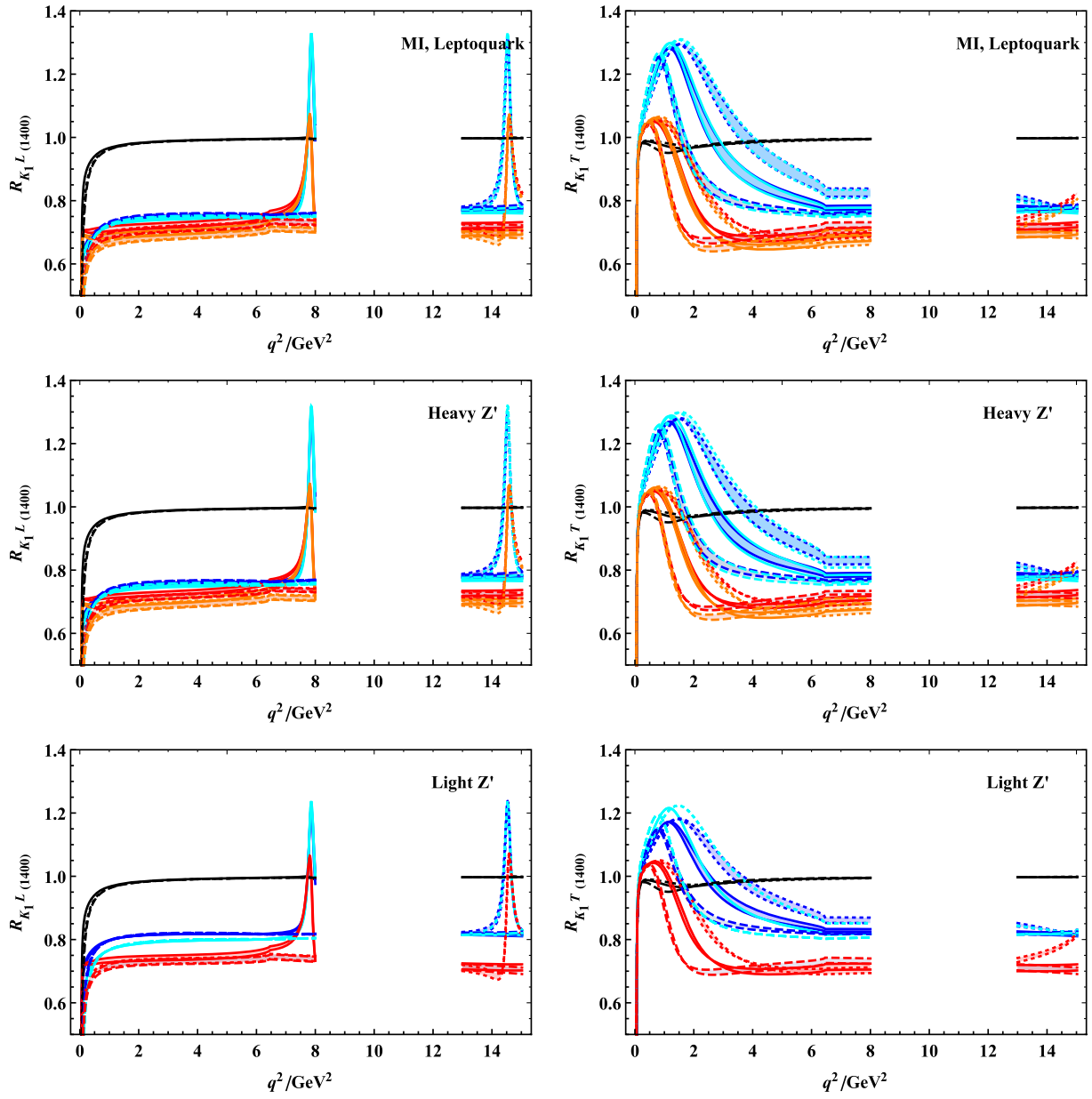

FIG. 4. Predictions for the polarized differential lepton universality ratio $R_{K_1^{L,T}(1400)}$ in the Standard Model, model-independent, leptoquark, heavy and light Z' models. The legends are same as in Fig. 1.

influence of NP. These observables against the square of the momentum transfer, q^2, are drawn in Figs. 1–4.

Our study shows that this analysis on one side is the complementary check of the $R_{K^{(*)}}$ anomalies in that such kind of anomalies could also be seen in R_{K_1}. On the other hand the observables $R_{K_1(1270,1400)}$ and $R_{K_1^{L,T}(1270,1400)}$ are found to be more interesting and sophisticated for the NP due to the involvement of the mixing angle θ_{K_1}. This analysis shows that in the NP scenarios and NP models under consideration, the results of $R_{K_1(1270)}$ are quite similar to R_{K^*} in the sense that they are lower than 1 in low q^2 region. This feature also holds for the longitudinal $R_{K^L(1270)}$, while in the same region the transverse $R_{K^T(1270)}$ are greater than 1, and particularly the ratios in scenario I (which can only be realized in Z' models) can reach 1.2 or even higher. All the unpolarized and polarized ratios for $K_1(1270)$ are shown to be insensitive to K_1 mixing angle θ_{K_1} and their values in the SM and in different NP scenarios (models) are distinguishable.

In addition, the results of $R_{K_1(1400)}$ and $R_{K_1^{L,T}(1400)}$ are more involved because these ratios are sensitive to not only the NP effects but also the K_1 mixing angle. Therefore to better study the NP effects via the

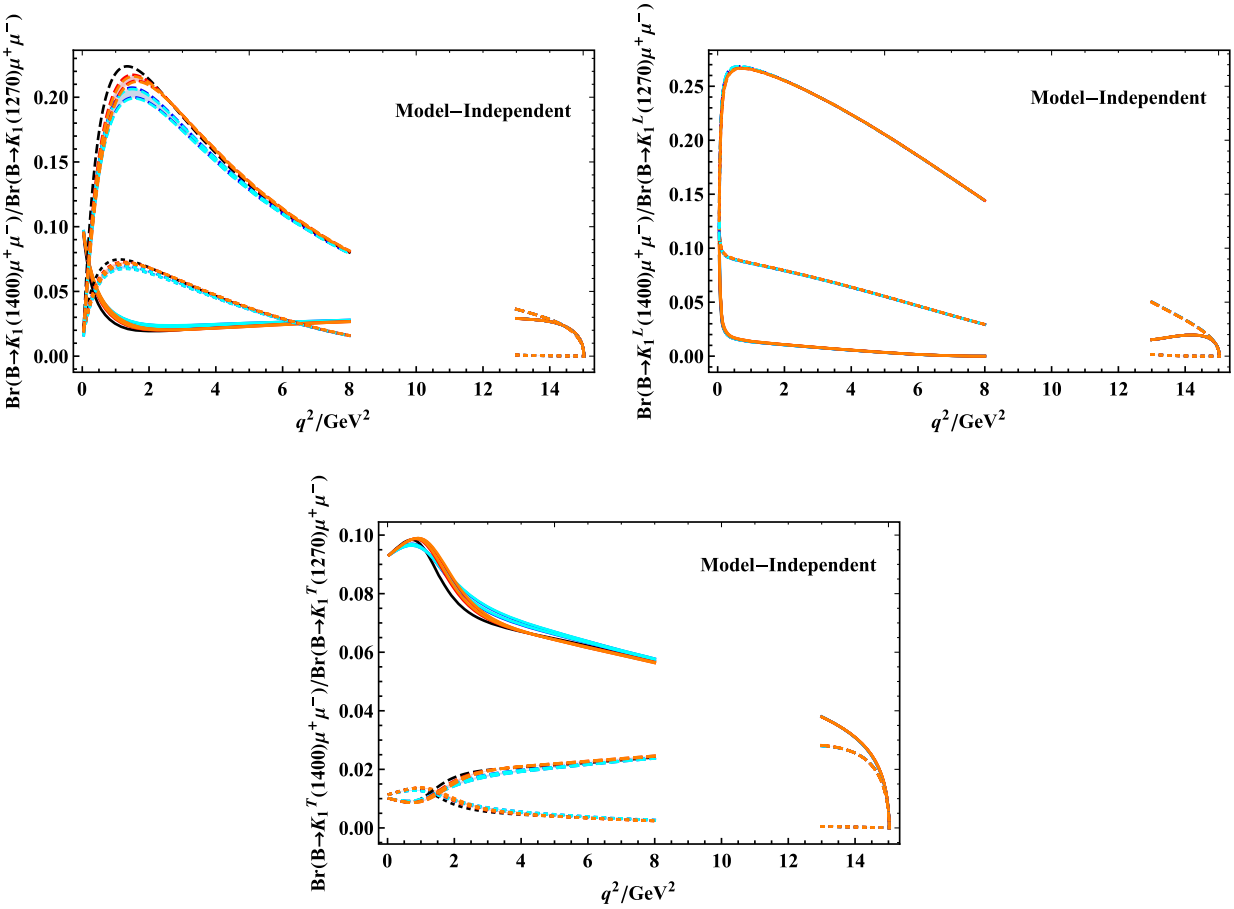

FIG. 5. Model-independent predictions for the ratio $R_\mu(K_1) = \mathcal{B}(B \to K_1(1400)\mu^+\mu^-)/\mathcal{B}(B \to K_1(1270)\mu^+\mu^-)$ for unpolarized and polarized K_1 in the model-independent scenarios. The legends are the same as in Fig. 1.

$R_{K_1^{(L,T)}(1400)}$, one essentially needs more precise value of θ_{K_1}. The most notable characteristic of LFU parameter for $K_1(1400)$ is probably that the $R_{K^L(1270)}$ can present a peak in medium q^2 region (below the resonance region) or high q^2 region, depending on the value of θ_{K_1}. As a complementary study of the NP, we also perform a study of the ratio $R_\mu(K_1)$, which are found to be insensitive to the NP effects from the NP scenarios (models) under consideration. This ratio can also be used to extract the precise value of the mixing angle θ_{K_1}. Therefore, if measurable, R_μ and $R_{K_1(1400)}$ can be complementary observables to determine the K_1 mixing angle and to test the leptoquark and Z' models.

In summary, the observables considered in the current study is not only important for the complementary check on the recently found $R_{K^{(*)}}$ anomalies but also useful to extract the information of the inherent mixing angle θ_{K_1}. Hence the precise measurements of $R_{K_1(1270,1400)}$ and $R_{K_1^{L,T}(1270,1400)}$ as well as R_μ in the current and the future colliders will be important for providing with insights of LFUV and as well to examine the leptoquark and Z' explanations of the $b \to s\mu^+\mu^-$ data.

ACKNOWLEDGMENTS

The authors would like to thanks Bhubanjyoti Bhattacharya for useful discussions on the NP parameters in the light Z' models. The authors would also like to thank Faisal Munir Bhutta for providing a source file for Wilson coefficents C_7^{eff} and C_9^{eff}. Two of the authors I. Ahmed and A. Paracha thank the hospitality provided by IHEP where most of the work is done. This work is partly supported by the National Natural Science Foundation of China (NSFC) with Grants No. 11521505 and No. 11621131001 and the China Postdoctoral Science Foundation with Grant No. 2018M631572.

APPENDIX: PREDICTIONS FOR R_{K_1} IN DIFFERENT BINS

In this Appendix, we present our predictions for $R_{K_1(1270,1400)}$ in the SM, the model-independent scenarios and the leptoquark and the Z' models. We show the results in different q^2 bins in Tables VII and VIII.

TABLE VII. SM and NP predictions for the LFU ratios $R_{K_1(1270)}$ in different bins. The errors are due to the errors of the best-fit Wilson coefficients.

Scenario	θ_{K_1}	q^2/GeV^2: [0.045,1]	q^2/GeV^2: [1,6]	q^2/GeV^2: [14,max]
SM	−34°	0.881	0.986	0.997
SM	−45°	0.882	0.986	0.997
SM	−57°	0.883	0.986	0.997
MI,I(A)	−34°	$0.782^{+0.004}_{-0.005}$	$0.780^{+0.006}_{-0.007}$	$0.775^{+0.004}_{-0.005}$
MI,I(A)	−45°	$0.796^{+0.004}_{-0.005}$	$0.783^{+0.006}_{-0.007}$	$0.775^{+0.004}_{-0.005}$
MI,I(A)	−57°	$0.811^{+0.005}_{-0.005}$	$0.788^{+0.007}_{-0.008}$	$0.775^{+0.004}_{-0.005}$
MI,LQ,II(A)	−34°	$0.751^{+0.001}_{-0.001}$	$0.708^{+0.008}_{-0.008}$	$0.719^{+0.009}_{-0.008}$
MI,LQ,II(A)	−45°	$0.764^{+0.002}_{-0.002}$	$0.708^{+0.008}_{-0.008}$	$0.719^{+0.009}_{-0.008}$
MI,LQ,II(A)	−57°	$0.778^{+0.002}_{-0.002}$	$0.708^{+0.008}_{-0.008}$	$0.720^{+0.009}_{-0.008}$
MI,I(B)	−34°	$0.779^{+0.004}_{-0.005}$	$0.773^{+0.006}_{-0.007}$	$0.767^{+0.004}_{-0.005}$
MI,I(B)	−45°	$0.793^{+0.004}_{-0.005}$	$0.777^{+0.006}_{-0.007}$	$0.767^{+0.004}_{-0.005}$
MI,I(B)	−57°	$0.809^{+0.005}_{-0.005}$	$0.782^{+0.007}_{-0.008}$	$0.767^{+0.004}_{-0.005}$
MI,LQ,II(B)	−34°	$0.740^{+0.001}_{-0.001}$	$0.684^{+0.008}_{-0.007}$	$0.695^{+0.008}_{-0.008}$
MI,LQ,II(B)	−45°	$0.753^{+0.001}_{-0.002}$	$0.684^{+0.007}_{-0.007}$	$0.695^{+0.008}_{-0.008}$
MI,LQ,II(B)	−57°	$0.769^{+0.002}_{-0.002}$	$0.684^{+0.007}_{-0.007}$	$0.695^{+0.008}_{-0.007}$
TeV Z',I(A)	−34°	$0.785^{+0.004}_{-0.004}$	$0.786^{+0.005}_{-0.006}$	$0.782^{+0.005}_{-0.006}$
TeV Z',I(A)	−45°	$0.798^{+0.004}_{-0.004}$	$0.790^{+0.006}_{-0.007}$	$0.782^{+0.004}_{-0.005}$
TeV Z',I(A)	−57°	$0.813^{+0.004}_{-0.004}$	$0.794^{+0.006}_{-0.007}$	$0.782^{+0.004}_{-0.005}$
TeV Z',II(A)	−34°	$0.754^{+0.001}_{-0.001}$	$0.714^{+0.005}_{-0.005}$	$0.724^{+0.008}_{-0.008}$
TeV Z',II(A)	−45°	$0.766^{+0.001}_{-0.001}$	$0.713^{+0.005}_{-0.005}$	$0.725^{+0.008}_{-0.008}$
TeV Z',II(A)	−57°	$0.780^{+0.001}_{-0.001}$	$0.713^{+0.005}_{-0.005}$	$0.725^{+0.008}_{-0.008}$
TeV Z',I(B)	−34°	$0.781^{+0.005}_{-0.006}$	$0.778^{+0.007}_{-0.009}$	$0.773^{+0.004}_{-0.005}$
TeV Z',I(B)	−45°	$0.795^{+0.006}_{-0.006}$	$0.781^{+0.008}_{-0.010}$	$0.773^{+0.004}_{-0.005}$
TeV Z',I(B)	−57°	$0.811^{+0.006}_{-0.006}$	$0.786^{+0.009}_{-0.011}$	$0.772^{+0.004}_{-0.005}$
TeV Z',II(B)	−34°	$0.742^{+0.001}_{-0.001}$	$0.688^{+0.008}_{-0.008}$	$0.698^{+0.008}_{-0.007}$
TeV Z',II(B)	−45°	$0.755^{+0.002}_{-0.002}$	$0.688^{+0.008}_{-0.008}$	$0.699^{+0.008}_{-0.007}$
TeV Z',II(B)	−57°	$0.770^{+0.002}_{-0.002}$	$0.688^{+0.008}_{-0.007}$	$0.699^{+0.008}_{-0.007}$
GeV Z',I(A)	−34°	$0.809^{+0.002}_{-0.002}$	$0.833^{+0.003}_{-0.004}$	$0.816^{+0.003}_{-0.004}$
GeV Z',I(A)	−45°	$0.819^{+0.002}_{-0.002}$	$0.836^{+0.004}_{-0.004}$	$0.816^{+0.003}_{-0.004}$
GeV Z',I(A)	−57°	$0.830^{+0.002}_{-0.003}$	$0.838^{+0.004}_{-0.005}$	$0.816^{+0.003}_{-0.004}$
GeV Z',II(A)	−34°	$0.764^{+0.001}_{-0.001}$	$0.727^{+0.008}_{-0.008}$	$0.708^{+0.010}_{-0.010}$
GeV Z',II(A)	−45°	$0.775^{+0.001}_{-0.002}$	$0.727^{+0.008}_{-0.007}$	$0.708^{+0.010}_{-0.010}$
GeV Z',II(A)	−57°	$0.788^{+0.002}_{-0.002}$	$0.727^{+0.008}_{-0.007}$	$0.708^{+0.010}_{-0.010}$
MeV Z',I(A)	−34°	0.788	0.816	0.816
MeV Z',I(A)	−45°	0.801	0.818	0.816
MeV Z',I(A)	−57°	0.815	0.822	0.816

TABLE VIII. SM and NP predictions for the LFU ratio $R_{K_1(1400)}$ in different bins. The errors are due to the errors in the best-fit results of the Wilson coefficients.

Scenario	θ_{K_1}	q^2/GeV^2: [0.045,1]	q^2/GeV^2: [1,6]	q^2/GeV^2: [13,max]
SM	−34°	0.887	0.984	0.993
SM	−45°	0.878	0.986	0.995
SM	−57°	0.875	0.986	0.995
MI,I(A)	−34°	$0.899^{+0.003}_{-0.003}$	$0.938^{+0.018}_{-0.018}$	$0.775^{+0.004}_{-0.005}$
MI,I(A)	−45°	$0.680^{+0.000}_{-0.000}$	$0.759^{+0.003}_{-0.004}$	$0.791^{+0.006}_{-0.006}$
MI,I(A)	−57°	$0.660^{+0.000}_{-0.001}$	$0.754^{+0.003}_{-0.004}$	$0.776^{+0.005}_{-0.006}$
MI,LQ,II(A)	−34°	$0.867^{+0.002}_{-0.002}$	$0.716^{+0.005}_{-0.005}$	$0.719^{+0.009}_{-0.008}$
MI,LQ,II(A)	−45°	$0.667^{+0.005}_{-0.005}$	$0.713^{+0.008}_{-0.008}$	$0.739^{+0.007}_{-0.006}$
MI,LQ,II(A)	−57°	$0.636^{+0.007}_{-0.007}$	$0.709^{+0.009}_{-0.008}$	$0.717^{+0.009}_{-0.008}$
MI,I(B)	−34°	$0.900^{+0.003}_{-0.003}$	$0.866^{+0.015}_{-0.016}$	$0.767^{+0.004}_{-0.005}$
MI,I(B)	−45°	$0.672^{+0.000}_{-0.001}$	$0.751^{+0.003}_{-0.004}$	$0.784^{+0.005}_{-0.006}$
MI,I(B)	−57°	$0.653^{+0.000}_{-0.001}$	$0.747^{+0.003}_{-0.004}$	$0.769^{+0.005}_{-0.006}$
MI,LQ,II(B)	−34°	$0.865^{+0.002}_{-0.002}$	$0.693^{+0.004}_{-0.004}$	$0.695^{+0.008}_{-0.007}$
MI,LQ,II(B)	−45°	$0.648^{+0.004}_{-0.004}$	$0.689^{+0.008}_{-0.007}$	$0.716^{+0.006}_{-0.006}$
MI,LQ,II(B)	−57°	$0.616^{+0.007}_{-0.006}$	$0.685^{+0.008}_{-0.008}$	$0.693^{+0.008}_{-0.008}$
TeV Z',I(A)	−34°	$0.899^{+0.003}_{-0.003}$	$0.871^{+0.013}_{-0.015}$	$0.782^{+0.004}_{-0.005}$
TeV Z',I(A)	−45°	$0.686^{+0.000}_{-0.000}$	$0.766^{+0.003}_{-0.004}$	$0.798^{+0.004}_{-0.005}$
TeV Z',I(A)	−57°	$0.667^{+0.000}_{-0.001}$	$0.762^{+0.003}_{-0.003}$	$0.783^{+0.004}_{-0.005}$
TeV Z',II(A)	−34°	$0.867^{+0.002}_{-0.002}$	$0.721^{+0.003}_{-0.003}$	$0.725^{+0.008}_{-0.008}$
TeV Z',II(A)	−45°	$0.671^{+0.003}_{-0.003}$	$0.718^{+0.006}_{-0.005}$	$0.744^{+0.006}_{-0.006}$
TeV Z',II(A)	−57°	$0.641^{+0.005}_{-0.005}$	$0.714^{+0.006}_{-0.006}$	$0.723^{+0.009}_{-0.008}$
TeV Z',I(B)	−34°	$0.900^{+0.004}_{-0.004}$	$0.868^{+0.019}_{-0.021}$	$0.773^{+0.004}_{-0.005}$
TeV Z',I(B)	−45°	$0.677^{+0.000}_{-0.001}$	$0.757^{+0.004}_{-0.005}$	$0.789^{+0.005}_{-0.005}$
TeV Z',I(B)	−57°	$0.658^{+0.000}_{-0.001}$	$0.752^{+0.004}_{-0.005}$	$0.774^{+0.004}_{-0.005}$
TeV Z',II(B)	−34°	$0.866^{+0.002}_{-0.002}$	$0.696^{+0.004}_{-0.005}$	$0.699^{+0.008}_{-0.007}$
TeV Z',II(B)	−45°	$0.651^{+0.005}_{-0.005}$	$0.693^{+0.008}_{-0.008}$	$0.719^{+0.006}_{-0.006}$
TeV Z',II(B)	−57°	$0.619^{+0.007}_{-0.007}$	$0.688^{+0.009}_{-0.008}$	$0.697^{+0.008}_{-0.008}$
GeV Z',I(A)	−34°	$0.893^{+0.002}_{-0.002}$	$0.891^{+0.009}_{-0.010}$	$0.818^{+0.003}_{-0.004}$
GeV Z',I(A)	−45°	$0.737^{+0.001}_{-0.002}$	$0.820^{+0.001}_{-0.002}$	$0.831^{+0.003}_{-0.004}$
GeV Z',I(A)	−57°	$0.722^{+0.002}_{-0.002}$	$0.817^{+0.001}_{-0.002}$	$0.819^{+0.003}_{-0.004}$
GeV Z',II(A)	−34°	$0.869^{+0.002}_{-0.002}$	$0.733^{+0.005}_{-0.005}$	$0.711^{+0.010}_{-0.009}$
GeV Z',II(A)	−45°	$0.687^{+0.004}_{-0.004}$	$0.733^{+0.008}_{-0.008}$	$0.732^{+0.008}_{-0.007}$
GeV Z',II(A)	−57°	$0.660^{+0.007}_{-0.006}$	$0.729^{+0.009}_{-0.008}$	$0.709^{+0.010}_{-0.010}$
MeV Z',I(A)	−34°	0.895	0.884	0.816
MeV Z',I(A)	−45°	0.690	0.800	0.830
MeV Z',I(A)	−57°	0.677	0.796	0.817

[1] Y. Li and C. D. L, Sci. Bull. **63**, 267 (2018).
[2] S. Bifani, S. Descotes-Genon, A. R. Vidal, and M. H. Schune, J. Phys. G **46**, 023001 (2019).
[3] J. P. Lees *et al.*, Phys. Rev. Lett. **109**, 101802 (2012).
[4] J. P. Lees *et al.*, Phys. Rev. D **88**, 072012 (2013).
[5] M. Huschle *et al.* (Belle Collaboration), Phys. Rev. D **92**, 072014 (2015).
[6] Y. Sato *et al.* (Belle Collaboration), Phys. Rev. D **94**, 072007 (2016).
[7] S. Hirose *et al.* (Belle Collaboration), Phys. Rev. Lett. **118**, 211801 (2017).

[8] R. Aaij *et al.* (LHCb Collaboration), Phys. Rev. Lett. **115**, 111803 (2015); **115**, 159901(E) (2015).
[9] R. Aaij *et al.* (LHCb Collaboration), Phys. Rev. Lett. **120**, 171802 (2018).
[10] R. Aaij *et al.* (LHCb Collaboration), Phys. Rev. D **97**, 072013 (2018).
[11] R. Aaij *et al.* (LHCb Collaboration), Phys. Rev. Lett. **120**, 121801 (2018).
[12] HFLAV Group, https://hflav-eos.web.cern.ch/hflav-eos/semi/summer18/RDRDs.html.
[13] J. Aebischer, J. Kumar, P. Stangl, and D. M. Straub, Eur. Phys. J. C **79**, 509 (2019).
[14] Z. R. Huang, Y. Li, C. D. Lu, M. A. Paracha, and C. Wang, Phys. Rev. D **98**, 095018 (2018).
[15] S. Fajfer, J. F. Kamenik, and I. Nisandzic, Phys. Rev. D **85**, 094025 (2012).
[16] X. Q. Li, Y. D. Yang, and X. Zhang, J. High Energy Phys. 08 (2016) 054.
[17] S. Iguro, T. Kitahara, Y. Omura, R. Watanabe, and K. Yamamoto, J. High Energy Phys. 02 (2019) 194.
[18] Y. Sakaki, M. Tanaka, A. Tayduganov, and R. Watanabe, Phys. Rev. D **88**, 094012 (2013).
[19] S. Jaiswal, S. Nandi, and S. K. Patra, J. High Energy Phys. 12 (2017) 060.
[20] R. Aaij *et al.* (LHCb Collaboration), Phys. Rev. Lett. **113**, 151601 (2014).
[21] R. Aaij *et al.* (LHCb Collaboration), J. High Energy Phys. 08 (2017) 055.
[22] B. Dey, Proc. Sci., ICHEP2018 (**2019**) 069, [arXiv:1811.11309].
[23] M. Bordone, G. Isidori, and A. Pattori, Eur. Phys. J. C **76**, 440 (2016).
[24] G. Hiller and F. Kruger, Phys. Rev. D **69**, 074020 (2004).
[25] A. K. Alok, B. Bhattacharya, A. Datta, D. Kumar, J. Kumar, and D. London, Phys. Rev. D **96**, 095009 (2017).
[26] A. K. Alok, B. Bhattacharya, D. Kumar, J. Kumar, D. London, and S. U. Sankar, Phys. Rev. D **96**, 015034 (2017).
[27] W. Altmannshofer, P. Stangl, and D. M. Straub, Phys. Rev. D **96**, 055008 (2017).
[28] J. Kumar, D. London, and R. Watanabe, Phys. Rev. D **99**, 015007 (2019).
[29] G. Hiller and I. Nisandzic, Phys. Rev. D **96**, 035003 (2017).
[30] B. Capdevila, A. Crivellin, S. Descotes-Genon, J. Matias, and J. Virto, J. High Energy Phys. 01 (2018) 093.
[31] F. Sala and D. M. Straub, Phys. Lett. B **774**, 205 (2017).
[32] M. Ciuchini, A. M. Coutinho, M. Fedele, E. Franco, A. Paul, L. Silvestrini, and M. Valli, Eur. Phys. J. C **77**, 688 (2017).
[33] W. Altmannshofer, C. Niehoff, P. Stangl, and D. M. Straub, Eur. Phys. J. C **77**, 377 (2017).
[34] A. K. Alok, A. Datta, A. Dighe, M. Duraisamy, D. Ghosh, and D. London, J. High Energy Phys. 11 (2011) 121.
[35] A. K. Alok, A. Datta, A. Dighe, M. Duraisamy, D. Ghosh, and D. London, J. High Energy Phys. 11 (2011) 122.
[36] L. Calibbi, A. Crivellin, and T. Ota, Phys. Rev. Lett. **115**, 181801 (2015).
[37] R. Alonso, B. Grinstein, and J. Martin Camalich, J. High Energy Phys. 10 (2015) 184.
[38] G. Hiller and M. Schmaltz, Phys. Rev. D **90**, 054014 (2014).
[39] B. Gripaios, M. Nardecchia, and S. A. Renner, J. High Energy Phys. 05 (2015) 006.
[40] I. de Medeiros Varzielas and G. Hiller, J. High Energy Phys. 06 (2015) 072.
[41] S. Sahoo and R. Mohanta, Phys. Rev. D **91**, 094019 (2015).
[42] S. Fajfer and N. Košnik, Phys. Lett. B **755**, 270 (2016).
[43] D. Bečirević, S. Fajfer, and N. Košnik, Phys. Rev. D **92**, 014016 (2015).
[44] D. Bečirević, N. Košnik, O. Sumensari, and R. Zukanovich Funchal, J. High Energy Phys. 11 (2016) 035.
[45] W. Altmannshofer, S. Gori, M. Pospelov, and I. Yavin, Phys. Rev. D **89**, 095033 (2014).
[46] A. Crivellin, G. D'Ambrosio, and J. Heeck, Phys. Rev. Lett. **114**, 151801 (2015).
[47] W. Altmannshofer and I. Yavin, Phys. Rev. D **92**, 075022 (2015).
[48] A. Crivellin, J. Fuentes-Martin, A. Greljo, and G. Isidori, Phys. Lett. B **766**, 77 (2017).
[49] I. Ahmed and A. Rehman, Chin. Phys. C **42**, 063103 (2018).
[50] M. Chala and M. Spannowsky, Phys. Rev. D **98**, 035010 (2018).
[51] W. Wang and S. Zhao, Chin. Phys. C **42**, 013105 (2018).
[52] R. Dutta, arXiv:1906.02412.
[53] H. Hatanaka and K. C. Yang, Phys. Rev. D **77**, 094023 (2008); **78**, 059902(E) (2008).
[54] H. Hatanaka and K. C. Yang, Phys. Rev. D **78**, 074007 (2008).
[55] M. A. Paracha, I. Ahmed, and M. J. Aslam, Eur. Phys. J. C **52**, 967 (2007).
[56] I. Ahmed, M. A. Paracha, and M. J. Aslam, Eur. Phys. J. C **54**, 591 (2008).
[57] I. Ahmed, M. A. Paracha, and M. J. Aslam, Eur. Phys. J. C **71**, 1521 (2011).
[58] A. Ahmed, I. Ahmed, M. A. Paracha, and A. Rehman, Phys. Rev. D **84**, 033010 (2011).
[59] S. Ishaq, F. Munir, and I. Ahmed, J. High Energy Phys. 07 (2013) 006.
[60] S. Ishaq, F. Munir, and I. Ahmed, Prog. Theor. Exp. Phys. **2016**, 013B02 (2016).
[61] R. H. Li, C. D. Lu, and W. Wang, Phys. Rev. D **79**, 094024 (2009).
[62] Y. Li, J. Hua, and K. C. Yang, Eur. Phys. J. C **71**, 1775 (2011).
[63] D. Du, A. X. El-Khadra, S. Gottlieb, A. S. Kronfeld, J. Laiho, E. Lunghi, R. S. Van de Water, and R. Zhou (Fermilab Lattice and MILC Collaborations), Phys. Rev. D **93**, 034005 (2016).
[64] M. Beneke, Th. Feldmann, and D. Seidel, Nucl. Phys. **B612**, 25 (2001).
[65] H. H. Asatryan, H. M. Asatrian, C. Greub, and M. Walker, Phys. Rev. D **65**, 074004 (2002).
[66] C. Greub, V. Pilipp, and C. Schupbach, J. High Energy Phys. 12 (2008) 040.
[67] R. Alonso, B. Grinstein, and J. M. Camalich, J. High Energy Phys. 10 (2015) 184.
[68] G. Hiller and M. Schmaltz, Phys. Rev. D **90**, 054014 (2014).
[69] S. Sahoo and R. Mohanta, Phys. Rev. D **91**, 094019 (2015).
[70] S. Fajfer and N. Konik, Phys. Lett. B **755**, 270 (2016).

[71] I. Ahmed and A. Rehman, Chin. Phys. C **42**, 063103 (2018).
[72] B. Bhattacharya, A. Datta, J. P. Guvin, D. London, and R. Watanabe, J. High Energy Phys. 01 (2017) 015.
[73] B. Bhattacharya, A. Datta, D. London, and S. Shivashankara, Phys. Lett. B **742**, 370 (2015).
[74] D. Buttazzo, A. Greljo, G. Isidori, and D. Marzocca, J. High Energy Phys. 11 (2017) 044.
[75] A. Angelescu, D. Bečirević, D. A. Faroughy, and O. Sumensari, J. High Energy Phys. 10 (2018) 183.
[76] G. Aad *et al.* (ATLAS Collaboration), Eur. Phys. J. C **76**, 5 (2016).
[77] R. Gauld, F. Goertz, and U. Haisch, Phys. Rev. D **89**, 015005 (2014).
[78] J. M. Cline, J. M. Cornell, D. London, and R. Watanabe, Phys. Rev. D **95**, 095015 (2017).
[79] A. Datta, J. Liao, and D. Marfatia, Phys. Lett. B **768**, 265 (2017).
[80] S. Raby and A. Trautner, Phys. Rev. D **97**, 095006 (2018).
[81] G. Hiller and M. Schmaltz, J. High Energy Phys. 02 (2015) 055.
[82] M. Tanabashi *et al.* (Particle Data Group), Phys. Rev. D **98**, 030001 (2018).